

# Dissolution of a multicomponent DNAPL pool in an experimental aquifer

Kenneth Y. Lee<sup>a,\*</sup>, Constantinos V. Chrysikopoulos<sup>b</sup>

<sup>a</sup> Department of Civil and Environmental Engineering, Rutgers, The State University of New Jersey, Piscataway, NJ 08854, USA

<sup>b</sup> Department of Civil Engineering, University of Patras, Patras 26500, Greece

Received 18 February 2005; received in revised form 30 July 2005; accepted 4 August 2005

Available online 3 October 2005

## Abstract

This paper presents the results from a well-defined, circular-shaped, multicomponent dense nonaqueous phase liquid (DNAPL) pool dissolution experiment conducted in a three-dimensional, bench scale model aquifer. The multicomponent pool is a mixture of tetrachloroethylene (PCE) and 1,1,2-trichloroethane (1,1,2-TCA); PCE was the major component and 1,1,2-TCA was the minor component. Downgradient plume concentrations were measured at five specific locations over time until the majority of the 1,1,2-TCA was depleted from the DNAPL pool source. The experimental results suggest distinct spatial-temporal plume patterns for minor DNAPL components versus major DNAPL components. The downgradient concentration varied over time for 1,1,2-TCA while a stable plume developed for PCE. A semi-analytical solution for contaminant transport resulting from dissolution of multicomponent nonaqueous phase liquid pools successfully simulated the plume structure and dynamics for both the major and minor DNAPL components.

© 2005 Elsevier B.V. All rights reserved.

**Keywords:** Groundwater pollution; Nonaqueous phase liquids; Dissolution; Contaminant transport; Mathematical models

## 1. Introduction

Subsurface formations are often polluted with nonaqueous phase liquid (NAPL) mixtures composed of more than one compound [1,2]. If the multicomponent NAPL mixture introduced to the subsurface is of sufficient quantity, the NAPL mixture will migrate downward to the groundwater table. Once the NAPL reaches the groundwater table, mixtures with specific gravity <1 (light nonaqueous phase liquids, or LNAPLs) form pools on top of the water table, whereas mixtures with specific gravity >1 (dense nonaqueous phase liquids, or DNAPLs) may keep migrating downward through the saturated zone and form pools on top of impermeable formations. Over time, components from the NAPL pool mixture slowly dissolve into the flowing interstitial water and create long-term groundwater contamination.

There are numerous studies on contaminant transport resulting from the dissolution of NAPL pools. Examples of recent published single-component pool dissolution studies include references [3–18] and examples of multicomponent NAPL pool dissolution studies include references [7,19–26].

For a dissolving multicomponent NAPL pool, the equilibrium solubility of each component varies with time because the mole fraction and the nonaqueous phase activity coefficient of each component changes as the pool composition changes [27,28]. Therefore, accounting for temporal changes in equilibrium solubility is essential for accurate analysis and prediction on the dissolution behavior of a multicomponent NAPL pool. However, due to factors such as slow dissolution rate and low aqueous solubility of typical NAPL compounds, it is difficult to observe changes in pool composition due to dissolution within a reasonable amount of experimental time. Without this type of experimental data, it would be difficult to validate multicomponent NAPL pool dissolution and solute transport mathematical models for fate and transport predictions. Hence, the objective of this study is

\* Corresponding author. Tel.: +1 732 445 2240.

E-mail addresses: kenlee@rci.rutgers.edu (K.Y. Lee), gios@upatras.gr (C.V. Chrysikopoulos).

**Nomenclature**

$A$	pool surface area ( $\text{cm}^2$ )
$C$	aqueous phase solute concentration ( $\text{mg/L}$ )
$C_b$	background aqueous phase solute concentration ( $\text{mg/L}$ )
$C_s$	aqueous saturation concentration ( $\text{mg/L}$ )
$C^w$	equilibrium aqueous solubility concentration ( $\text{mg/L}$ )
$d$	pool thickness ( $\text{cm}$ )
$D$	molecular diffusion coefficient ( $\text{cm}^2/\text{h}$ )
$D_e$	effective molecular diffusion coefficient, equal to $D/\tau^*$ ( $\text{cm}^2/\text{h}$ )
$D_x$	longitudinal hydrodynamic dispersion coefficient ( $\text{cm}^2/\text{h}$ )
$D_y$	lateral hydrodynamic dispersion coefficient ( $\text{cm}^2/\text{h}$ )
$D_z$	hydrodynamic dispersion coefficient in the vertical direction ( $\text{cm}^2/\text{h}$ )
$f_{oc}$	organic carbon fraction of the porous medium
$k$	time and space dependent local mass transfer coefficient ( $\text{cm}/\text{h}$ )
$k^*$	time-invariant average mass transfer coefficient ( $\text{cm}/\text{h}$ )
$\bar{k}$	average mass transfer coefficient ( $\text{cm}/\text{h}$ )
$K_d$	distribution coefficient ( $\text{L}/\text{kg}$ )
$K_{oc}$	organic carbon partition coefficient ( $\text{L}/\text{kg}$ )
$l_x$	pool length along the longitudinal direction ( $\text{cm}$ )
$l_{x_0}, l_{y_0}$	$x$ and $y$ Cartesian coordinates of the pool origin ( $\text{cm}$ )
$m_f$	total number of pulses
$M$	number of moles remaining in the pool ( $\text{mol}$ )
$M^0$	initial number of moles in the pool ( $\text{mol}$ )
$p$	component number indicator
$P$	total number of components in the nonaqueous phase
$r$	radius of circular pool ( $\text{cm}$ )
$R$	dimensionless retardation factor
$t$	time ( $\text{h}$ )
$U_x$	average interstitial velocity ( $\text{cm}/\text{h}$ )
$x, y, z$	spatial coordinates ( $\text{cm}$ )
$X$	dimensionless nonaqueous phase mole fraction.

**Greek letters**

$\alpha_L, \alpha_T$	longitudinal and transverse dispersivity, respectively ( $\text{cm}$ )
$\gamma$	dimensionless nonaqueous phase activity coefficient
$\theta$	aquifer porosity (liquid volume/aquifer volume)
$\lambda$	decay coefficient ( $1/\text{h}$ )
$\mu$	dummy integration variable

$\rho_b$	sand bulk density ( $\text{kg}/\text{L}$ )
$\tau$	dummy integration variable
$\tau^*$	tortuosity factor ( $\geq 1$ ).

to observe and describe comprehensively contaminant plume evolution of one component in a multicomponent DNAPL pool dissolution experiment. To achieve this objective, a two-component mixture, namely tetrachloroethylene (PCE) and 1,1,2-trichloroethane (1,1,2-TCA), is selected as the DNAPL pool source. A small initial mole fraction of 0.36% for 1,1,2-TCA is selected such that the contaminant plume evolution can be comprehensively observed within a reasonable amount of experimental time. The multicomponent DNAPL pool dissolution experiment is performed in a three-dimensional, bench scale, homogeneous model aquifer. Downgradient aqueous phase samples are collected and analyzed at various times from five predetermined sampling locations within the experimental aquifer. The dissolution experiment continued until majority of the 1,1,2-TCA was depleted from the pool source.

**2. Experimental setup and aquifer characteristics**

A schematic diagram of the experimental aquifer is shown in Fig. 1. The experimental aquifer is a rectangular glass tank with internal dimensions of 150.0 cm in length, 40.0 cm in height, and 21.6 cm in width. The glass thickness is 0.95 cm. A circular flat pool with exact DNAPL–water interfacial area is formed by removing a circular disk of radius  $r = 3.8$  cm and pool cavity thickness of  $d = 0.5$  cm from an aluminum sheet that was placed at the bottom of the aquifer (see bottom of Fig. 1). The aluminum plate was hard anodized to avoid corrosion, and the pool bottom was covered with a thin Teflon sheet. Holes (0.2 cm diameter) were drilled into the Teflon sheet 1.0 cm apart in the form of a square matrix and a glass bead (0.5 cm diameter) was placed on top of each hole. A circular #60 stainless steel mesh was placed on top of the glass beads to prevent sand settling into the pool cavity. The pool void volume is approximately 12 mL. The delivery of the DNAPL mixture into the pool was accomplished through a stainless steel tube that was inserted into the pool through a horizontal hole drilled into the aluminum plate.

A Plexiglas sampling plate was constructed to allow precise positioning of sampling needles within the three-dimensional aquifer. A schematic diagram of the sampling plate and its placement location with respect to the circular DNAPL pool is shown in the upper portion of Fig. 1. The sampling nodes consist of 16 columns by 7 rows of 0.08 cm diameter holes positioned on a regular 5 cm  $\times$  2.5 cm grid. Aqueous samples are collected from the experimental aquifer using 20 gauge, stainless steel luer-hub needles (Hamilton,

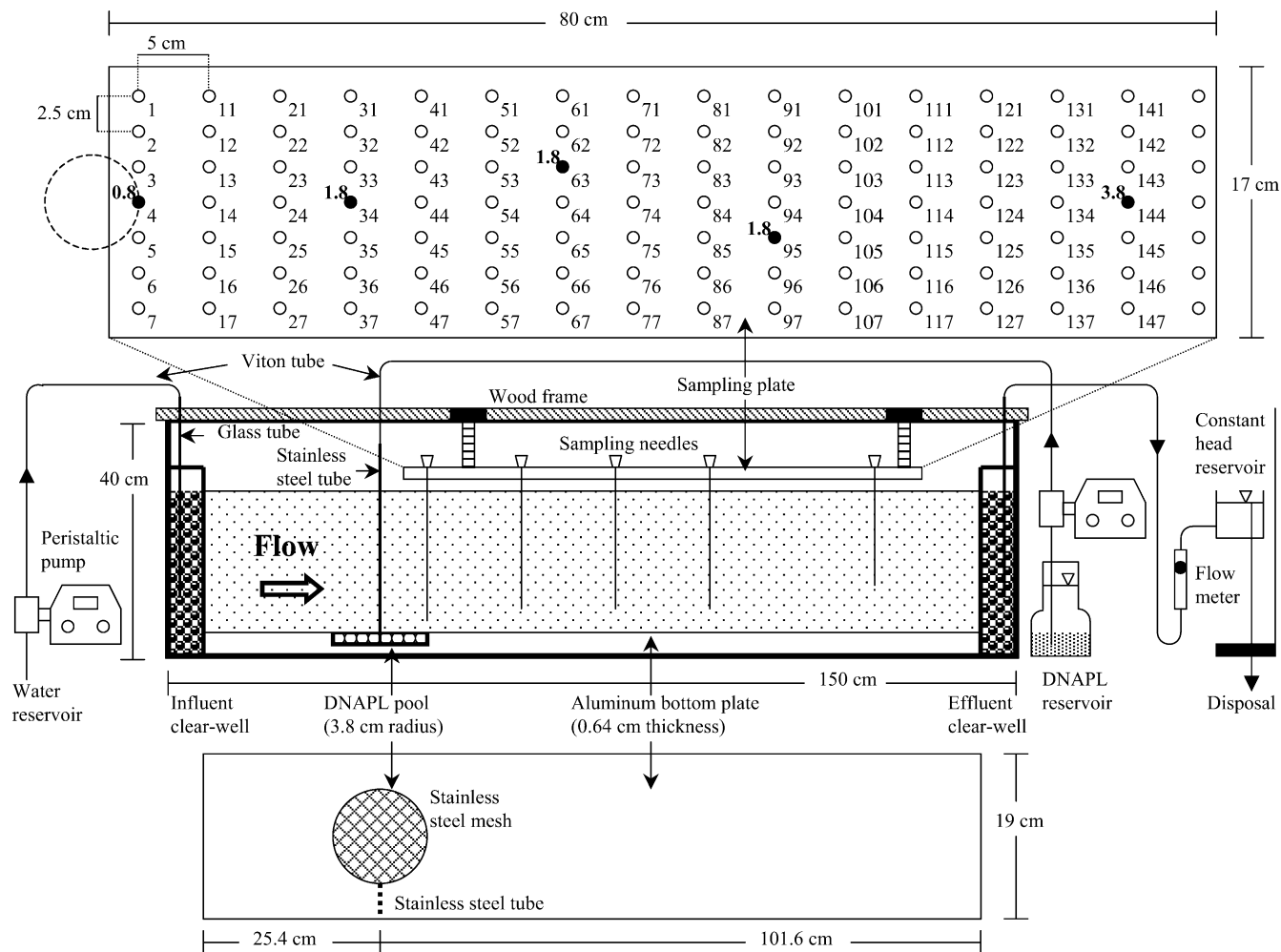


Fig. 1. Schematic diagram of the experimental aquifer. Filled circles on the sampling plate represent actual needle placement locations. For each filled circle, the lower right number indicates the sampling port number and the upper left bold numbers indicate the needle placement depth measured in cm from the bottom of the aquifer.

Reno, Nevada). Sampling needles were vertically inserted into the aquifer and their locations are indicated on the sampling plate (Fig. 1) as filled circles. For each filled circle shown on the sampling plate, the lower right number indicates the node number and the upper left bold number represents the needle placement depth measured in cm from the bottom of the aquifer.

The experimental aquifer was packed with kiln dried Monterey sand (RMC Lonestar, Monterey, CA) that passed the #40 sieve (0.425 mm) and retained on the #60 sieve (0.250 mm). The sand was packed in 1–2 cm lifts to a total depth of about 15 cm. Each lift of sand was packed under a 5 cm water head and a mechanical vibrating device was employed to obtain uniform packing. The horizontal flow was accomplished by pumping degassed, deionized water into the influent clear well while maintaining constant head at the effluent clear well. The experimental aquifer was placed inside a constant temperature chamber (Forma Scientific, Marietta, OH) maintained at 20 °C. The works of [10,17]

provide an in-depth discussion on the design and construction of the model aquifer and details of a conservative tracer study to determine aquifer characteristics.

### 3. Dissolution experiment

The average interstitial velocity within the experimental aquifer was maintained at  $U_x = 1.5$  cm/h. An aqueous solution containing approximately 200 mg/L of sodium azide was delivered into the influent clear well. The addition of sodium azide inhibited biological degradation of PCE and 1,1,2-TCA.

A 50 mL graduated cylinder was used to prepare the multi-component DNAPL mixture. Prior to adding any chemicals, 10 mL of deionized water was poured into the graduated cylinder. Next, approximately 12 mL of PCE and 0.04 mL of 1,1,2-TCA was injected below the water level into the graduated cylinder. The water behaved as a cap to prevent

volatilization of the DNAPL. Gas chromatograph (GC) analysis of the DNAPL mixture confirmed a PCE mole fraction of 99.64% and a 1,1,2-TCA mole fraction of 0.36%. The pool dissolution experiment was initiated by pumping the multi-component DNAPL mixture through the stainless steel tube into the pool at a rate of 3 mL/min. The pump was on for 4 min until all of the DNAPL mixture was delivered into the pool cavity.

A total of nine sampling sessions were conducted at progressive times after the initiation of the dissolution process. For each sampling session, interstitial liquid samples are collected from sampling needles at nodes 4, 34, 63, 95, and 144 (see Fig. 1). Each sample was collected using a 1 mL disposable tuberculin syringe (Becton Dickinson & Co., NJ). Approximately 0.1 mL of the interstitial fluid was purged and discarded from the sampling needle just before a 0.3 mL liquid sample collection. Each water sample was analyzed using a GC according to the analytical method described by [10].

#### 4. Mathematical modeling

The transient transport of each dissolving component originating from a NAPL pool in a three-dimensional homogeneous porous medium under steady-state uniform flow conditions is governed by [29]:

$$\begin{aligned} R_p \frac{\partial C_p(t, x, y, z)}{\partial t} &= D_{x_p} \frac{\partial^2 C_p(t, x, y, z)}{\partial x^2} + D_{y_p} \frac{\partial^2 C_p(t, x, y, z)}{\partial y^2} \\ &+ D_{z_p} \frac{\partial^2 C_p(t, x, y, z)}{\partial z^2} - U_x \frac{\partial C_p(t, x, y, z)}{\partial x} \\ &- \lambda_p R_p C_p(t, x, y, z), \end{aligned} \quad (1)$$

where  $C$  is the aqueous phase solute concentration;  $R$  the dimensionless retardation factor;  $D_x, D_y, D_z$  the longitudinal, lateral, and vertical hydrodynamic dispersion coefficients, respectively;  $U_x$  the average interstitial fluid velocity;  $\lambda$  a first-order decay constant;  $x, y, z$  the spatial coordinates in the longitudinal, lateral, and vertical directions, respectively;  $t$  the time; and subscript  $p$  is the component number indicator. It is assumed that each dissolved component is sorbing under local equilibrium conditions. The decay term  $\lambda RC$  in the governing Eq. (1) indicates that the total concentration of a component (aqueous plus sorbed solute mass) may diminish due to possible biological/chemical degradation.

For a circular-shaped, multicomponent NAPL pool with constant vertical thickness and homogeneous composition, the appropriate initial and boundary conditions for each dissolving component are:

$$C_p(0, x, y, z) = C_{b_p}, \quad (2)$$

$$C_p(t, \pm\infty, y, z) = C_{b_p}, \quad (3)$$

$$C_p(t, x, \pm\infty, z) = C_{b_p}, \quad (4)$$

$$\begin{aligned} -D_{e_p} \frac{\partial C_p(t, x, y, 0)}{\partial z} &= \begin{cases} \bar{k}_p(t)[C_p^w(t) - C_{b_p}] & (x - l_{x_0})^2 + (y - l_{y_0})^2 \leq r^2, \\ 0 & \text{otherwise,} \end{cases} \end{aligned} \quad (5)$$

$$C_p(t, x, y, \infty) = C_{b_p}, \quad (6)$$

where  $C_b = 0$  is the background aqueous phase concentration of the dissolved component;  $C^w$  the equilibrium aqueous solubility concentration that is time-dependent because the mole fraction of each component in the pool is changing as the NAPL dissolves into the aqueous phase;  $D_{e_p} = D_p/\tau^*$  is the effective molecular diffusion coefficient for component  $p$  (where  $D$  is the molecular diffusion coefficient; and  $\tau^* \geq 1$  is the tortuosity coefficient);  $\bar{k}(t) = k(t, x, y)$  is the average mass transfer coefficient applicable for the entire NAPL–water interface (where  $k(t, x, y)$  is the local mass transfer coefficient dependent on time and location on the NAPL–water interface) [7]; and  $l_{x_0}$  and  $l_{y_0}$  indicate the  $x$  and  $y$  Cartesian coordinates of the center of circular pool, respectively. It should be noted that boundary condition (5) indicates that the diffusive flux into the concentration boundary layer at the NAPL–water interface is governed by Fick's law and is equal to the convective mass transfer flux.

For a dissolving multicomponent mixture, the equilibrium aqueous solubility is defined for each component as [27]:

$$C_p^w(t) = C_{s_p} X_p(t) \gamma_p(X_p), \quad (7)$$

where  $C_s$  is the pure component saturation concentration (solubility);  $X$  the nonaqueous phase mole fraction; and  $\gamma$  is the nonaqueous phase activity coefficient that depends on the mole fraction of component  $p$  in the nonaqueous phase. It should be noted that for an ideal solution  $\gamma_p = 1$  and Eq. (7) reduces to Raoult's law:

$$C_p^w(t) = C_{s_p} X_p(t). \quad (8)$$

The number of moles of each component present in the nonaqueous phase as a function of time is given by:

$$X_p(t) = \frac{M_p(t)}{\sum_{p=1}^P M_p(t)} \quad (p = 1, 2, \dots, P), \quad (9)$$

where  $P$  is the total number of components in the nonaqueous phase;  $M_p(t)$  the number of moles of component  $p$  present in the nonaqueous phase at time  $t$  given by [7,30]:

$$M_p(t) = M_p^{\bullet} - \sum_{m=1}^{m_f} \frac{\bar{k}_p(t) C_p^w(t_m) A \theta \Delta t_m}{(\text{mol wt})_p} \quad (t \geq \Delta t_m), \quad (10)$$

where  $M_p^{\bullet}$  is the initial number of moles of component  $p$  in the nonaqueous phase;  $A$  the NAPL–water interfacial area;  $\theta$  the

aquifer porosity;  $m$  a summation index;  $m_f$  an integer indicating the total number of time steps (or pulses);  $t_m$  the sampling time (e.g.  $t_1 = 27$  h,  $t_2 = 120$  h, ...); and  $\Delta t_m = t_m - t_{m-1}$  is the time interval of the  $m$ th pulse.

A closed-form analytical solution to the physical problem described by the governing partial differential Eq. (1) subject to initial and boundary conditions (2)–(6) cannot be derived, because  $C^w(t)$  and  $\bar{k}(t)$ , which both appear in the source boundary condition (5), are time dependent parameters. An analytical solution to this problem has been derived for the case of a single-component NAPL pool, representing the limiting case where  $C^w(t) = C_s$  and  $\bar{k}(t) = k^*$ , where  $k^*$  is a time-invariant average mass transfer coefficient [29]. For the multicomponent pool described in this study, the semi-analytical solution presented by [7] is modified as follows:

$$C_p(t, x, y, z) = \sum_{m=1}^{m_f} \bar{k}_p(t_m) [C_p^w(t_m) - C_{b_p}] [\Phi_p(t - t_{m-1}, x, y, z) - \Phi_p(t - t_m, x, y, z)] + [C_p^w(t_{m_f}) - C_{b_p}] \times \Phi_p(t - t_{m_f}, x, y, z) \quad (t > t_{m_f}), \quad (11)$$

where

$$\Phi_p(t, x, y, z) = \frac{1}{2\pi D_{e_p}} \int_0^t \int_{\mu_1}^{\mu_2} \left( \frac{D_{z_p}}{R_p \tau} \right)^{1/2} \exp \left[ -\lambda_p \tau - \frac{R_p z^2}{4D_{z_p} \tau} \right] \times \exp[-\mu^2] (\text{erf}[n_2] - \text{erf}[n_1]) d\mu d\tau, \quad (12)$$

$$\mu_1 = (y - l_{y_0} + r) \left( \frac{R_p}{4D_{y_p} \tau} \right)^{1/2}, \quad (13)$$

$$\mu_2 = (y - l_{y_0} - r) \left( \frac{R_p}{4D_{y_p} \tau} \right)^{1/2}, \quad (14)$$

$$n_1 = \left\{ x - \frac{U_x \tau}{R_p} - l_{x_0} + [r^2 - (v - l_{y_0})^2]^{1/2} \right\} \times \left( \frac{R_p}{4D_{x_p} \tau} \right)^{1/2}, \quad (15)$$

$$n_2 = \left\{ x - \frac{U_x \tau}{R_p} - l_{x_0} - [r^2 - (v - l_{y_0})^2]^{1/2} \right\} \times \left( \frac{R_p}{4D_{x_p} \tau} \right)^{1/2}, \quad (16)$$

$$v = y - \mu \left( \frac{4D_{y_p} \tau}{R_p} \right)^{1/2}, \quad (17)$$

where  $\mu$  and  $\tau$  are dummy integration variables. It should be noted that in (11) the superposition principle is employed over the time interval  $\Delta t$ . Superposition is possible because the governing Eq. (1) is linear with respect to the liquid phase solute concentration. The semi-analytical solution assumes that the source input can be represented as a summation of consecutive pulse-type boundary conditions, with NAPL pool composition, and consequently  $C^w$  and  $\bar{k}$ , of each component to remain constant over a “small” time interval,  $\Delta t_m$ . It should be noted that the accuracy of the semi-analytical solution presented increases with decreasing pulse time interval [7].

## 5. Estimation of model parameters

The retardation factor,  $R$ , is determined for each NAPL component based on the following equation for linear, reversible sorption [31]:

$$R_p = 1 + \frac{\rho_b}{\theta} K_{d_p}, \quad (18)$$

where  $\rho_b$  is the aquifer bulk density and  $K_{d_p}$  is the distribution coefficient. It should be noted that in this study PCE and 1,1,2-TCA are indicated as the first ( $p = 1$ ) and second ( $p = 2$ ) component, respectively. It should also be noted that Eq. (18) assumes that the sorption behavior of one component is unaffected by the sorption behavior of another component. The distribution coefficient can be estimated for each component from the correlation [32]:

$$K_{d_p} = f_{oc} K_{oc_p}, \quad (19)$$

where  $f_{oc}$  is the organic carbon fraction of the porous medium and  $K_{oc}$  is the organic carbon partition coefficient.

The organic carbon fraction of the porous medium is  $f_{oc} = 6.35 \times 10^{-4}$ , the aquifer bulk density is  $\rho_b = 1.61$  kg/L, and the aquifer porosity is  $\theta = 0.415$  [10]. The organic carbon partition coefficients for PCE and 1,1,2-TCA used in this study are  $K_{oc_1} = 363.08$  L/kg and  $K_{oc_2} = 69.98$  L/kg, respectively [33]. Consequently, in view of Eqs. (18) and (19), the retardation factors for PCE and 1,1,2-TCA are calculated to be  $R_1 = 1.89$  and  $R_2 = 1.17$ , respectively.

The hydrodynamic dispersion coefficients are determined using the following relationships:

$$D_{x_p} = \alpha_L U_x + D_{e_p}, \quad (20)$$

$$D_{y_p} = D_{z_p} = \alpha_T U_x + D_{e_p}, \quad (21)$$

where  $\alpha_L$  and  $\alpha_T$  are the longitudinal and transverse aquifer dispersivities. The dispersivity values associated with this study are  $\alpha_L = 0.259$  cm and  $\alpha_T = 0.019$  cm [10] and a tortuosity coefficient for sand of  $\tau^* = 1.43$  is considered [34]. The molecular diffusion coefficients used in this study are  $D_1 = 0.0313$  cm<sup>2</sup>/h and  $D_2 = 0.0333$  cm<sup>2</sup>/h [21]. Therefore, the calculated hydrodynamic dispersion coefficients

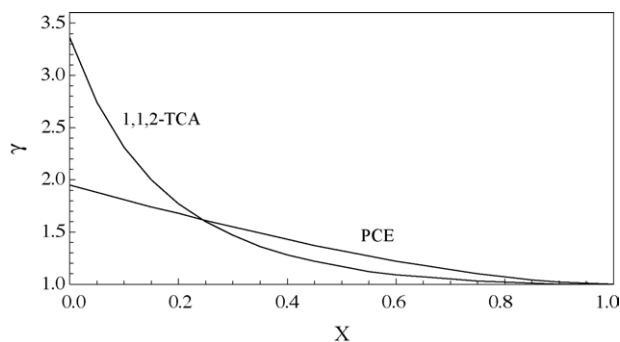


Fig. 2. UNIFAC derived nonaqueous phase activity coefficients as a function of nonaqueous phase mole fraction for a mixture of PCE and 1,1,2-TCA (adopted from [21]).

are  $D_{x_1} = 0.410 \text{ cm}^2/\text{h}$ ,  $D_{y_1} = D_{z_1} = 0.050 \text{ cm}^2/\text{h}$ ,  $D_{x_2} = 0.412 \text{ cm}^2/\text{h}$ , and  $D_{y_2} = D_{z_2} = 0.052 \text{ cm}^2/\text{h}$ .

The nonaqueous phase activity coefficients can be obtained using the UNIFAC method [35]. Fig. 2 shows the UNIFAC derived nonaqueous phase activity coefficients as a function of nonaqueous phase mole fraction for a mixture of PCE and 1,1,2-TCA. For this study, the nonaqueous phase mole fraction of PCE ranges from an initial mole fraction of  $X_1(0) = 99.64\%$  to near 100% toward the end of the dissolution experiment, and for 1,1,2-TCA the nonaqueous phase mole fraction ranges from  $X_2(0) = 0.36\%$  to near 0% toward the end of the dissolution experiment. Because of the small range in mole fraction variation, the UNIFAC derived nonaqueous phase activity coefficients for PCE and 1,1,2-TCA can be assumed to be a constant for the entire duration of the experiment equal to  $\gamma_1 = 1.0$  and  $\gamma_2 = 3.3$ . The pure component saturation concentrations for the two components are  $C_{s_1} = 150 \text{ mg/L}$  and  $C_{s_2} = 4400 \text{ mg/L}$  [33]. Therefore, the calculated initial equilibrium aqueous solubilities are  $C_1^w(0) = 149.5 \text{ mg/L}$  and  $C_2^w(0) = 53.6 \text{ mg/L}$ .

## 6. Results and discussion

The observed aqueous phase contaminant concentrations from all sampling sessions are graphically shown in Fig. 3. The highest DNAPL concentrations were observed at sampling node 4, which is the closest sampling location to the DNAPL pool. Conversely, the lowest concentrations, in general, were observed at sampling node 144, which is farthest away from the pool source. For each set of aqueous phase contaminant concentrations collected (at a specific sampling time), the corresponding value of  $\bar{k}_p$  is estimated by fitting the semi-analytical solution (Eq. (11)) to the experimental data using the non-linear least squares regression program PEST [36]. The average mass transfer coefficients for the two components were estimated to be  $\bar{k}_1 = 0.0453 \text{ cm/h}$  and  $\bar{k}_2 = 0.0454 \text{ cm/h}$ , for all nine data sets collected during the entire duration of the dissolution experiment. The

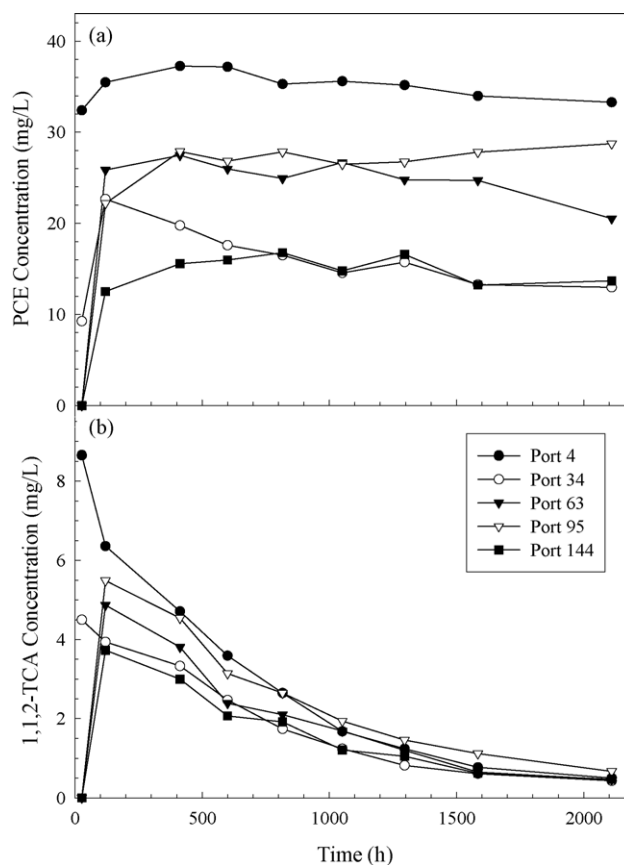


Fig. 3. Observed aqueous phase DNAPL concentrations as a function of time for: (a) PCE and (b) 1,1,2-TCA.

fitted mass transfer coefficients are time invariant because for the experimental design of this study the DNAPL–water interfacial area is maintained constant. However, for a shrinking DNAPL pool the mass transfer coefficient is expected to be time-dependent [7,29]. For the special case of a non-shrinking single-component pool in a two-dimensional, homogeneous aquifer, where the aqueous phase contaminant concentration is non-decaying, the following analytical expression for the mass transfer coefficient has been derived [15]:

$$k^* = 2D_e \left( \frac{U_x}{\pi D_z l_x} \right)^{1/2}, \quad (22)$$

where  $l_x$  is the pool length along the longitudinal direction. Note that all the variables in Eq. (22) associated with this study are constants. The calculated time-invariant average mass transfer coefficients using Eq. (22) are  $k_1^* = 0.049 \text{ cm/h}$  and  $k_2^* = 0.050 \text{ cm/h}$ . The mass transfer coefficients approximated by the relatively simple expression (22) are very similar to the corresponding coefficients determined from the experimental multicomponent pool dissolution data collected in this study. It should be noted that, according to Eq. (22), the mass transfer coefficient varies for each component as the values of  $D_e$  and  $D_z$  are component dependent. It should also

be noted that PCE and 1,1,2-TCA have similar properties. Therefore, it is expected that these two compounds would generate similar mass transfer coefficients.

As the DNAPL mixture dissolves into the interstitial water of the experimental aquifer, the mole fraction of 1,1,2-TCA decreases over time, which results in a considerably lower equilibrium aqueous solubility concentration. The equilibrium aqueous phase concentrations as a function of time for PCE and 1,1,2-TCA are plotted in Fig. 4a and the nonaqueous phase mole fraction as a function of time for 1,1,2-TCA ( $X_2$ ) is plotted in Fig. 4b. Note that the PCE nonaqueous phase mole fraction at any time is simply  $X_1 = 1 - X_2$ . Figs. 5 and 6 present the observed dissolved concentrations as well as the simulated concentration profiles for PCE and 1,1,2-TCA, respectively, along the centerline of the aquifer in the  $x$ - $z$  plane at progressing sampling times. The solid circles represent sampling locations and the bold numbers indicate observed concentrations. The pool center is located at  $x = -3.8$  cm. It should be noted that the PCE concentration contours in Fig. 5 appear to reach a steady-state after  $t > 120$  h and subsequent simulated concentration contours are all identical. The concentration profiles for 1,1,2-TCA presented in Fig. 6 show very interesting plume evolution. Note that 1,1,2-TCA concentration increases at early times but the plume size decrease as the multicomponent pool dissolves into the experimental aquifer and the 1,1,2-TCA component is depleted from the pool. Figs. 5 and 6 demonstrate that the semi-analytical solution (11) describing contami-

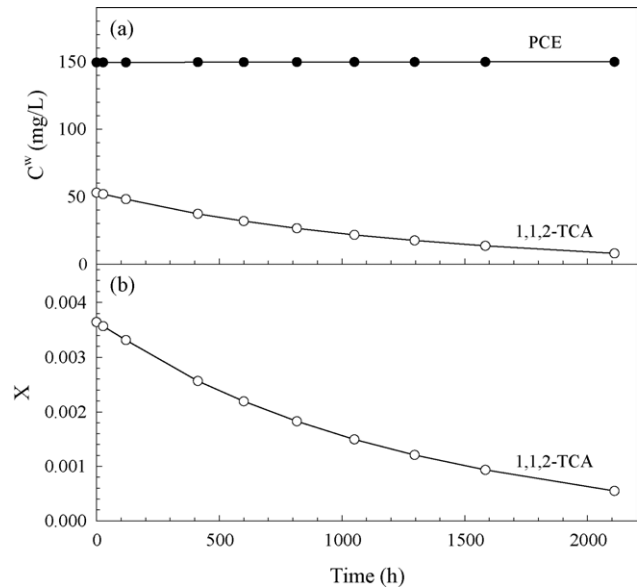


Fig. 4. (a) Estimated equilibrium aqueous-phase concentration as a function of time for PCE and 1,1,2-TCA and (b) the nonaqueous phase mole fraction as a function of time for 1,1,2-TCA.

nant transport from a dissolving multicomponent NAPL pool in a three-dimensional, homogeneous porous medium under steady-state uniform flow, simulated the experimental data for both PCE and 1,1,2-TCA components of the pool.

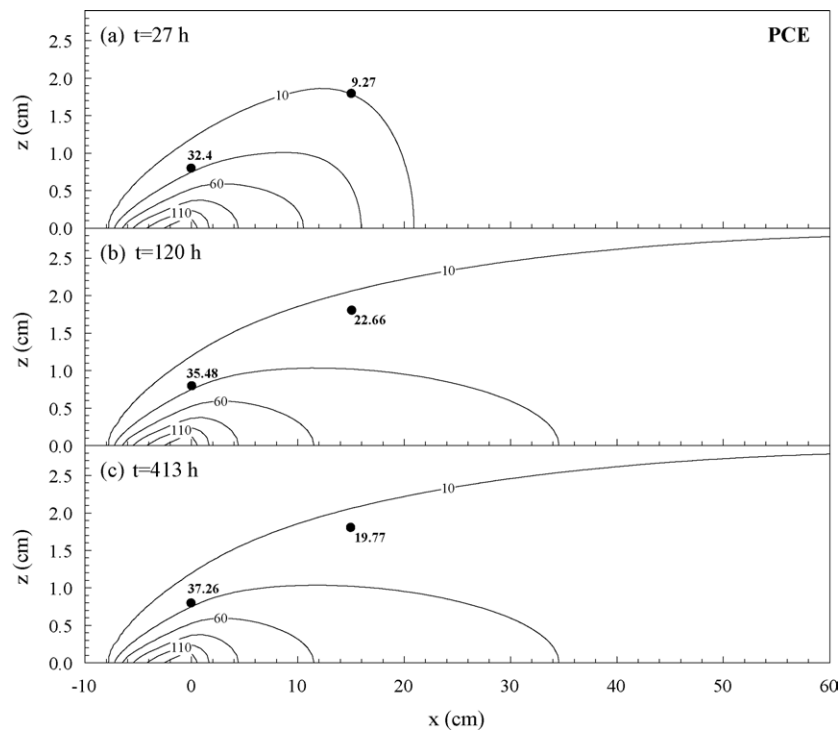


Fig. 5. Simulated PCE concentration contour plots (mg/L), along the centerline of the aquifer in the  $x$ - $z$  plane for (a)  $t = 27$  h, (b)  $t = 120$  h, and (c)  $t = 413$  h since the initiation of the dissolution process. The solid circles represent sampling locations and the bold numbers indicate observed concentrations. The pool center is located at  $x = -3.8$  cm and the contour intervals are 25 mg/L.

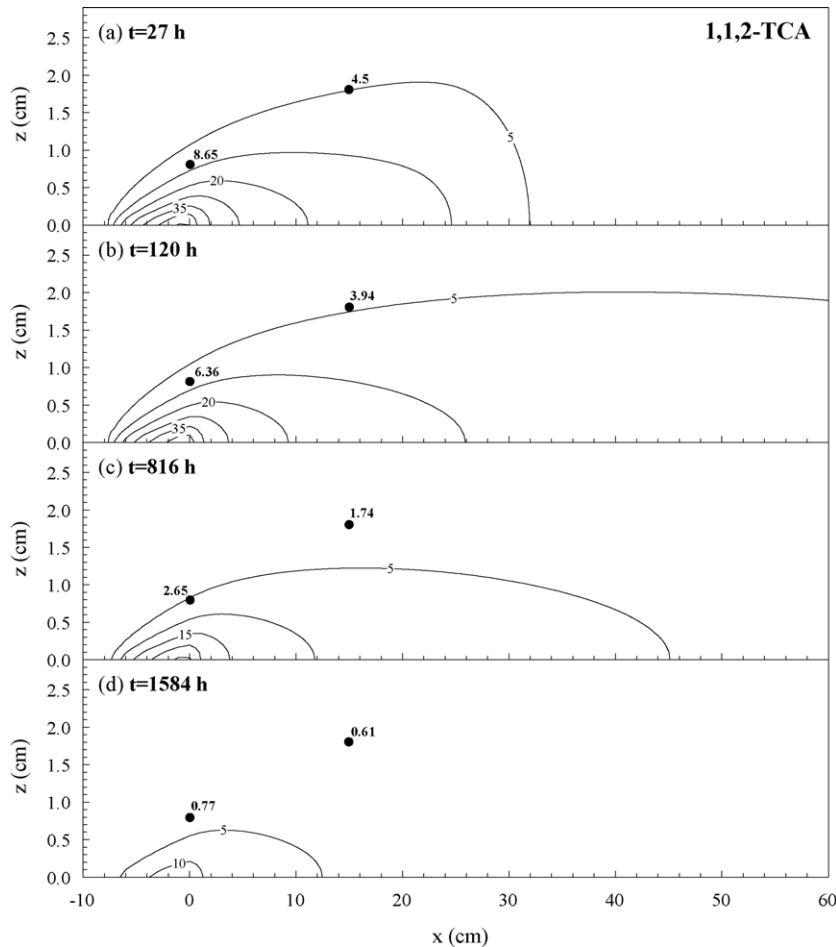


Fig. 6. Simulated 1,1,2-TCA concentration contour plots (mg/L), along the centerline of the aquifer in the  $x$ - $z$  plane for (a)  $t = 27$  h, (b)  $t = 120$  h, (c)  $t = 816$  h, and (d)  $t = 1584$  h since the initiation of the dissolution process. The solid circles represent sampling locations and the bold numbers indicate observed concentrations. The pool center is located at  $x = -3.8$  cm. The contour intervals are 7.5 mg/L for (a and b), and 5 mg/L for (c and d).

## 7. Summary

A three-dimensional multicomponent DNAPL pool dissolution experiment was conducted in a bench-scale, homogeneous model aquifer. A flat circular-shaped pool with exact DNAPL–water interfacial area was formed through a specially designed bottom plate. The multicomponent mixture consists of PCE and 1,1,2-TCA with initial mole fractions of 99.64 and 0.36%, respectively. Aqueous phase samples are collected from five different downgradient locations at nine progressively increasing dissolution times.

For this study, we observed that a decrease in aqueous phase concentration for the minor component (1,1,2-TCA) while the aqueous phase concentrations for the major component (PCE) remained relatively constant over time. The fitted average mass transfer coefficients for both of the DNAPL pool components were approximately equal ( $\bar{k}_1(t) = 0.0453$  cm/h,  $\bar{k}_2(t) = 0.0454$  cm/h) and time invariant due to the experimental design of a non-shrinking multicomponent DNAPL pool used in the present study. The semi-analytical solution for multicomponent pool dissolution presented in

this work was found to describe both PCE and 1,1,2-TCA plumes well.

## Acknowledgements

This research was sponsored by the Environmental Protection Agency, under Grant No. R-823579-01-0. However, the manuscript has not been subjected to the Agency's peer and administrative review, and therefore, does not necessarily reflect the views of the Agency and no official endorsement should be inferred.

## References

- [1] P.B. Bedient, H.S. Rifai, C.J. Newell, *Ground Water Contamination, Transport and Remediation*, second ed., Prentice Hall, Upper Saddle River, NJ, 1999.
- [2] C. Khachikian, T.C. Harmon, *Transp. Porous Media* 38 (2000) 3.
- [3] M.R. Anderson, R.L. Johnson, J.F. Pankow, *Environ. Sci. Technol.* 26 (1992) 901.

- [4] R.L. Johnson, J.F. Pankow, *Environ. Sci. Technol.* 26 (1992) 896.
- [5] C.V. Chrysikopoulos, E.A. Voudrias, M.M. Fyrrillas, *Transp. Porous Media* 16 (1994) 125.
- [6] E.A. Seagren, B.E. Rittmann, A.J. Valocchi, *Environ. Sci. Technol.* 28 (1994) 833.
- [7] C.V. Chrysikopoulos, K.Y. Lee, *J. Contam. Hydrol.* 31 (1998) 1.
- [8] T.-J. Kim, C.V. Chrysikopoulos, *Water Resour. Res.* 35 (1999) 449.
- [9] C.V. Chrysikopoulos, T.-J. Kim, *Transp. Porous Media* 38 (2000) 167.
- [10] C.V. Chrysikopoulos, K.Y. Lee, T.C. Harmon, *Water Resour. Res.* 36 (2000) 1687.
- [11] F.J. Leij, M.Th. van Genuchten, *Transp. Porous Media* 38 (2000) 141.
- [12] A. Sciortino, T.C. Harmon, W.W.G. Yeh, *Water Resour. Res.* 36 (2000) 1723.
- [13] M.E. Tatalovich, K.Y. Lee, C.V. Chrysikopoulos, *Transp. Porous Media* 38 (2000) 93.
- [14] E.T. Vogler, C.V. Chrysikopoulos, *Stochastic Environ. Res. Risk Assess.* 15 (2001) 33.
- [15] C.V. Chrysikopoulos, P.-Y. Hsuan, M.M. Fyrrillas, *Water Resour. Res.* 38 (2002) 1026.
- [16] B.K. Dela Barre, T.C. Harmon, C.V. Chrysikopoulos, *Water Resour. Res.* 38 (2002) 1133.
- [17] K.Y. Lee, C.V. Chrysikopoulos, *Water Res.* 36 (2002) 3911.
- [18] W.M.J. Bao, E.T. Vogler, C.V. Chrysikopoulos, *Environ. Geol.* 43 (2003) 968.
- [19] K.Y. Lee, C.V. Chrysikopoulos, *Environ. Geol.* 26 (1995) 157.
- [20] H.-Y.N. Holman, I. Javandel, *Water Resour. Res.* 32 (1996) 915 (Correction, *Water Resour. Res.* 32 (1996) 1917).
- [21] K.Y. Lee, C.V. Chrysikopoulos, *J. Environ. Eng. ASCE* 124 (1998) 851.
- [22] E.A. Seagren, B.E. Rittmann, A.J. Valocchi, *J. Contam. Hydrol.* 37 (1999) 111.
- [23] C. Eberhardt, P. Grathwohl, *J. Contam. Hydrol.* 59 (2002) 45.
- [24] J.W. Roy, J.E. Smith, R.W. Gillham, *J. Contam. Hydrol.* 59 (2002) 163.
- [25] E.A. Seagren, T.O. Moore, *J. Environ. Eng. ASCE* 129 (2003) 786.
- [26] K.Y. Lee, *J. Environ. Eng. ASCE* 130 (2004) 1507.
- [27] S. Banerjee, *Environ. Sci. Technol.* 18 (1984) 587.
- [28] J.E. McCray, P.J. Dugan, *Water Resour. Res.* 38 (2002) 1097.
- [29] C.V. Chrysikopoulos, *Water Resour. Res.* 31 (1995) 1137.
- [30] K.Y. Lee, *Environ. Geol.* 43 (2002) 132.
- [31] I. Hashimoto, K.B. Deshpande, H.C. Thomas, *Ind. Eng. Chem. Fund.* 3 (1964) 213.
- [32] S.W. Karickhoff, D.S. Brown, T.A. Scott, *Water Res.* 24 (1979) 241.
- [33] D. Mackay, W.Y. Shiu, K.C. Ma, *Illustrated Handbook of Physical-chemical Properties and Environmental Fate for Organic Chemicals Volatile Organic Chemicals*, vol. 3, Lewis Publishers, Chelsea, MI, 1992.
- [34] G. de Marsily, *Quantitative Hydrogeology, Groundwater Hydrology for Engineers*, Academic Press, San Diego, CA, 1986.
- [35] A. Fredenslund, J. Gmehling, P. Rasmussen, *Vapor-liquid Equilibria Using UNIFAC*, Elsevier, New York, 1977.
- [36] J. Doherty, L. Brebber, P. Whyte, *PEST: Model-Independent Parameter Estimation*, Watermark Computing, Brisbane, Australia, 1994.